EES Catalysis

PAPER

View Article Online
View Journal

Cite this: DOI: 10.1039/d6ey00029k

Phenothiazine redox mediators boost photocatalytic hydrogen evolution

Daniel Baumgarten, [a] Marco Gollasch, [a] Yesleen Gupta, [c] Moritz Jahn, [c] Alexander K. Mengele, [b] Sven Rau, [bd] Carsten Streb [c] and Birgit Esser *[ad]

The photocatalytic production of green hydrogen constitutes an important step towards sustainable energy storage. An ambitious goal is to couple reductive and oxidative photocatalysis, *i.e.*, the hydrogen-evolution reaction (HER) with water oxidation to achieve overall water splitting. Herein, we explore a pathway towards such coupled processes by using phenothiazines (PTs) as redox mediators (RMs) in HER. In this work, we explored the reductive half reaction utilizing a new hybrid SED-RM architecture with a photocatalytic system consisting of the thiomolybdate cluster $(NH_4)_2[Mo_3S_{13}]$ as catalyst, ascorbic acid as sacrificial electron donor, and $[Ru(bpy)_3](PF_6)_2$ (bpy = 2,2′-bipyridine) as photosensitiser (PS). We show that the catalytic performance of the system is improved by a factor of three (increase in turnover number (TON) from 6760 to 20 660 and in turnover frequency (TOF) from 1130 h^{-1} to 3440 h^{-1} (for 6h)) with 10*H*-phenothiazine (**PTH**) as RM. Stern–Volmer experiments show that **PTH** and derivatives effectively quench the excited state of $[Ru(bpy)_3](PF_6)_2$ – independent of pH – enabling photocatalytic HER to be performed at the lower pH of 2.55, where the catalyst is more active due to a higher availability of protons. A near-linear correlation between the emission quenching ability of the PT derivatives and the photocatalytic performance suggests the initial reductive quenching step to be an important kinetic factor in the catalytic cycle. Our study proposes RMs as a strategy to boost the performance of photocatalytic HER systems by mediating efficient electron transfers even at low pH values and paves the way towards coupled reductive and oxidative photocatalysis.

Received 9th February 2026,
Accepted 12th March 2026

DOI: 10.1039/d6ey00029k

rsc.li/eescatalysis

Broader context

The conversion of solar to chemical energy is one of the most promising research fields to provide carbon-neutral, sustainable energy. "Green" hydrogen formed by light-driven proton reduction is a key energy carrier in artificial photosynthesis. However, artificial photocatalysis suffers from several intrinsic problems, namely the use of sacrificial donors forming chemical waste, and their pH window of operation lying higher than ideal for proton reduction. We herein propose redox mediators in hydrogen-evolution-reaction photocatalysis that enable operation at lower pH values and set the stage for coupling oxidative and reductive photocatalysis. Specifically, we find that phenothiazines can act as potent, pH-independent reductive quenchers for the ruthenium-based photosensitizer $[Ru(bpy)_3]^{2+}$. This allows for the photocatalytic system to be operated at a lower pH value <3, enhancing the catalytic performance of the thiomolybdate cluster $(NH_4)_2[Mo_3S_{13}]$ by a factor of three. This work illustrates on how using suitable redox mediators can enhance photocatalytic efficiency and possibly enable a coupling of catalytic cycles, as phenothiazines can form stable radical cations whose vacancies could be filled by electron equivalents originating from an oxidative catalytic cycle.

Introduction

Artificial photosynthesis, *i.e.* the conversion of solar to chemical energy, is one of the most promising research fields to provide carbon-neutral, sustainable energy.[1–4] Specifically, "green" hydrogen formed by light-driven proton reduction is a key energy carrier in artificial photosynthesis schemes. Over the last years, the impact of hydrogen on the energy sector has been increasing, with the demand estimated to lie between 500 and 800 million metric tons per year by 2050.[5] The production of green hydrogen

[a] *Institute of Organic Chemistry II and Advanced Materials, Ulm University, Albert-Einstein-Allee 11, 89081 Ulm, Germany. E-mail: birgit.esser@uni-ulm.de, www.esserlab.com*
[b] *Institute of Inorganic Chemistry I, Ulm University, Albert-Einstein-Allee 11, 89081 Ulm, Germany*
[c] *Department of Chemistry, Johannes Gutenberg University Mainz, Duesbergweg 10–14, 55128 Mainz, Germany*
[d] *CELEST Green Energy Lab Ulm, Ulm University, Lise-Meitner-Str. 16, 89081 Ulm, Germany*

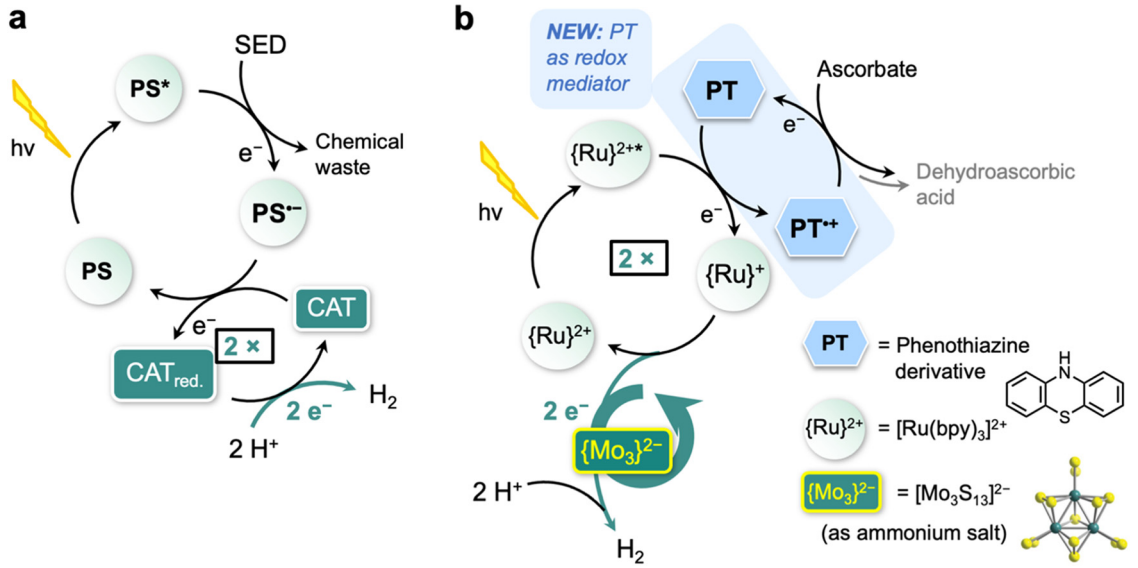

Fig. 1 (a) Schematic representation of a three-component photocatalytic HER system featuring the reductive quenching pathway of the photoexcited photosensitizer (PS*), followed by electron transfer to the catalyst (CAT) that initiates hydrogen generation; (b) schematic representation using phenothiazines (PTs) as a redox mediator (RM) in the $(NH_4)_2[Mo_3S_{13}]$ (=$\{Mo_3\}^{2-}$)-catalyzed HER with $[Ru(bpy)_3]^{2+}$ ($\{Ru\}^{2+}$) as PS.

using renewable energy or photocatalytic processes represents the most environmentally friendly approach[6] in the pursuit of sustainable and versatile energy sources. Therefore, the photocatalytic reductive hydrogen-evolution reaction (HER) has emerged as active research field, with the first reports dating back to Lehn and Sauvage from the late 1970s.[7] Consecutively, many systems for HER-photocatalysis have been developed.[8–13] In general, photocatalytic HER systems typically contain three components, as illustrated in Fig. 1a: A photosensitizer (PS), a catalyst (CAT) and a sacrificial electron donor (SED). In this three-component system, upon light absorption, the PS forms an excited state PS*, which is then reductively quenched by the SED. The CAT is a species that can undergo a reversible reduction and features active sites capable of protonation/hydride formation. These active sites are responsible for the hydrogen formation. The SED is required to provide the electrons that are necessary for the reductive catalysis.[14–16]

An ambitious goal is to couple reductive and oxidative processes, *i.e.*, HER with water oxidation, in order to achieve overall water splitting. This also mimics biological photosynthesis, where the two Photosystems II and I are coupled *via* cytochrome b_6f (complexes embedded in the thylakoid membrane) to enable directional electron transfer from water to $NADP^+$.[17,18] To achieve this, the electrons necessary for HER must be provided from the respective coupled oxidative process. In the currently most common HER system, however, the electrons are provided by an SED, which thereafter decomposes to form chemical waste. If an oxidative catalysis is to be coupled to HER to provide electrons, one pathway could be to use a redox mediator (RM) which can reversibly transfer electrons without undergoing irreversible degradation.

We herein set out to investigate the feasibility of this approach by employing 10*H*-phenothiazine (**PTH**) into the HER catalytic cycle as RM (Fig. 1b). Given success for the reductive half reaction (HER), this study could set ground for a potential coupling of catalytic half-reactions, *i.e.* oxidative and reductive catalysis. This could lead to the removal of the SED within the catalysis on the reductive cycle, as well as the sacrificial electron acceptor in the oxidative cycle in future studies. Phenothiazines (PTs) find application in various fields, *i.e.* in battery (solid) electrodes[19] or (redox-flow)[20–22] batteries and in charge-transfer-emitters[23,24] and are known for their ability to form (relatively) stable oxidized states. This, as well as their synthetic tuneability, is the basis for their ample use as organic electrode materials in batteries.[25] PTs have been explored in reductive photocatalysis on few occasions, demonstrating an enhancement in catalytic activity.[26–29]

As HER-photocatalytic system we chose one using the thiomolybdate cluster $(NH_4)_2[Mo_3S_{13}]$ ($(NH_4)_2\{Mo_3\}$).[30] This CAT is of significant interest due to its high HER activity.[31] For light-driven HER, the CAT can be combined with the well-established $[Ru(bpy)_3]^{2+}$ ($\{Ru\}^{2+}$, bpy = 2,2′-bipyridine) complex as PS and ascorbic acid (HAsc) as SED (Fig. 1b).[31] The reactivity and stability of $\{Mo_3\}^{2-}$ under the given reaction conditions has been reported previously. Theoretical and experimental data showed that the catalyst is stable under reductive conditions and undergoes a series of activation/deactivation steps based on exchange of the terminal disulfide ligands with solvent ligands, resulting in speciation in solution.[31,32] By employing PT RMs, we show that the catalytic performance of the system is improved by a factor of three with an increase in turnover number (TON) from 6760 to 20 660. However, in this system the usage of the SED as terminal electron source still leads to the formation of dehydroascorbic acid as waste product. Stern–Volmer experiments show that **PTH** and its derivatives effectively quench the excited state of $\{Ru\}^{2+}$ – independent of pH – and thereby enable photocatalytic HER to

be performed at the quite low pH of 2.55, where CAT is more active. We observe a near-linear correlation between the emission quenching ability of the respective PT derivative and the photocatalytic performance of the system, which suggests the initial quenching step to be an important kinetic factor in the catalytic cycle.

Results and discussion

We first tested the ability of **PTH** to quench the photoexcited state of the PF_6-salt of $\{Ru\}^{2+}$ (in MeOH : H_2O (9 : 1, v : v) based on previously reported conditions[33]). With a Stern–Volmer quenching constant of *ca.* $K_{SV\text{-}PTH}$ = 1200 M^{-1} (50 eq.), **PTH** is an efficient quencher (Fig. 2a). Even more importantly, **PTH** efficiently quenches the PS, regardless of the pH value of the solution, measured from pH = 0.7–13.5, making it particularly attractive for enabling photocatalytic HER at lower pH values. Durrant *et al.* and Artero *et al.* showed that HER and the here used $\{Mo_3\}^{2-}$ CAT performs best at acidic (low) pH (pH = 0), since this accelerates the protonation step of the reduced CAT.[16,34] In contrast, the typically used SED HAsc quenches best at higher pH values (*i.e.* pH 4), as the ascorbate ion (Asc^-) is easier to oxidize than HAsc (pK_a(HAsc) = 4.1).[16] Since the SED is responsible for the start of the electron cascade, this renders the optimal operating pH value for these systems to be at pH 4.[33] In this work, the initial reductive quenching step of the excited Ru-PS at lower pH (pH < 4) values is done by the added RM **PTH**. This removes the necessity of an ascorbate-ion to collide with the excited state leading to the reductively quenched PS $\{Ru\}^+$, ultimately lowering the needed concentration of ascorbate and making catalysis feasible at a lower pH value. In addition to a pH-independent quenching, **PTH** already quenches efficiently at lower concentrations (50 eq.) relative to the PS (corresponding to a concentration of 1 mM), while for HAsc in the literature often higher concentrations are used, *i.e.* 10 mM[33] corresponding to 500 eq. relative to PS. This opens the field to perform HER catalysis at a lower pH value, while still maintaining good reductive quenching of the excited PS to facilitate the start of the electron cascade.

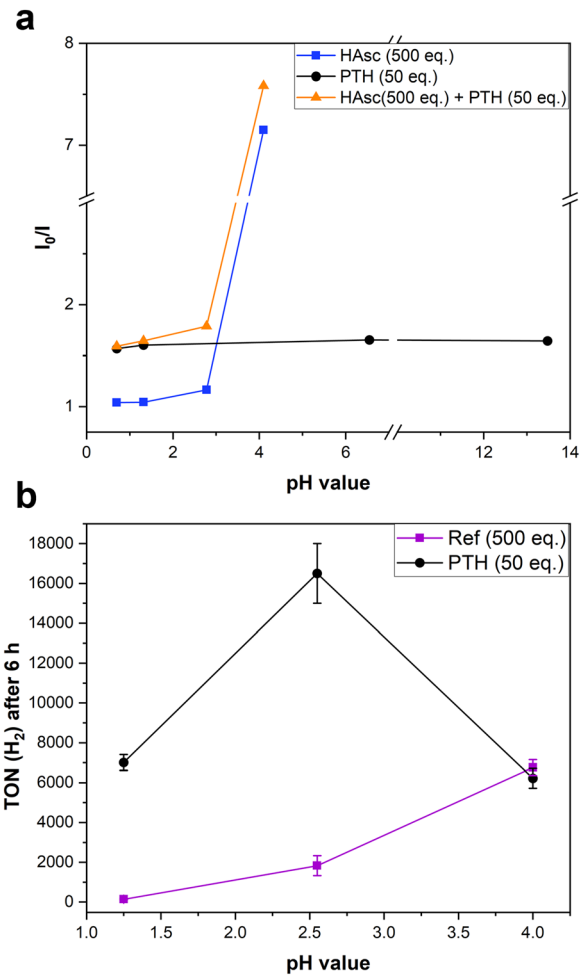

Fig. 2 (a) Excited-state quenching ability of **PTH**, HAsc and a **PTH**/HAsc mixture towards photoexcited $\{Ru\}^{2+}$ at different pH values in MeOH : H_2O (9 : 1, v : v) (I_0: emission intensity before addition of a quencher, I: emission intensity after addition of the respective quencher equivalents). (b) Averaged TONs of H_2 after 6 h at different pH values without ("Ref") and with **PTH** ("PTH") as RM (1 mM [50 eq. to PS]) (with 0.3 μM $(NH_4)_2\{Mo_3\}$, 20 μM $\{Ru\}^{2+}$, 10 mM HAsc [500 eq. to PS] in MeOH : H_2O (9 : 1, v : v)), irradiation at 455 nm).

Regarding a possible competition between PS excited-state quenching by **PTH** *vs.* HAsc or Asc^-, using a mixture of HAsc (500 eq.) and **PTH** (50 eq., each relative to PS) provides roughly the added values obtained for each individual quencher in the emission quenching (I_0/I_{PTH}(pH 6.55) = 1.65; I_0/I_{HAsc} (pH 2.78) = 1.17; $I_0/I_{PTH+HAsc}$(pH 2.78) = 1.79) with Stern–Volmer quenching constants of $K_{SV\text{-}PTH}$ = 1200 M^{-1}, $K_{SV\text{-}HAsc}$ = 34 M^{-1} (pH 2.78) and $K_{SV\text{-}HAsc}$ = 1230 M^{-1} (pH 4). This implies that their quenching happens independently (Fig. 2a).

The quenching of the excited state of the $\{Ru\}^{2+}$ PS by **PTH** is of reductive nature *via* an electron transfer (ET) to form $\{Ru\}^+$ (Fig. S12). A possible energy transfer (triplet–triplet Dexter energy transfer (TTEnT)) can be ruled out as the ^{3}MLCT energy of $\{Ru\}^{2+}$ (2.08 eV as PF_6 salt)[35] is lower than the corresponding T_1 state of similar PTs, as shown by Sartor *et al.* ($E_{00,T1}$ = 2.34 eV),[36] making TTEnT endergonic. This is further supported by femtosecond transient-absorption (fs-TA) measurements on covalently linked PT-Ru dyads and triads showing the formation of the radical cation $PT^{\bullet+}$.[29,37–39]

We next explored **PTH** in photocatalytic HER using $\{Ru\}^{2+}$ as PS and $(NH_4)_2\{Mo_3\}$ as CAT, according to a procedure by Heiland *et al.*[33] The (reference) photocatalytic system contained $\{Ru\}^{2+}$ (20 μM, as PF_6 salt), $\{Mo_3\}^{2-}$ (0.3 μM as ammonium salt), HAsc (10 mM) as SED at different pH values, and MeOH : H_2O (9 : 1, v : v) as solvent. In experiments with **PTH** as RM, it was added in 1 mM concentration (50 eq. relative to PS). We used a ventilated modular open-source photoreactor, published by Kowalczyk *et al.*[40] and equipped with an LED (λ_{max} = 455 nm, $P \approx 40$ mW cm^{-2}), with experiments carried out at (21 ± 1) °C (for temperature dependency of the catalytic system see SI, Fig. S7) in triplicate with error bars shown in the graphs. Hydrogen formation was quantified after a time period of 6 h using headspace gas chromatography. Control experiments showed no

hydrogen evolution without irradiation, or when $\{Mo_3\}^{2-}$, $\{Ru\}^{2+}$ or HAsc were absent.[31] In addition, measurements with **PTH** (1 mM) and in the absence of the SED showed no hydrogen evolution after a period of 6 h.

At pH 4 as the optimal pH for the reference system (using aqueous NH_4OH to adjust the pH value[33]), an average TON of 6220 is obtained with **PTH** and of 6760 without **PTH**, confirming that at this pH the concentration of Asc^- is high enough to efficiently quench photoexcited $\{Ru\}^{2+}$ itself. At lower pH, on the other hand, the TONs of the reference system with HAsc as SED fall to 1830 (pH 2.55) and 140 (pH 1.25), while the TONs with added **PTH** sharply rise to an average 16 500 at pH 2.55 and remain high at pH 1.25 with a TON of 7010 (*cf.* Table 2, the pH was adjusted using H_3PO_4 as acid or NaOH or NH_4OH as base). It is remarkable that **PTH** significantly increases the activity of the HER photocatalytic system by enabling photocatalysis to be performed at lower pH (with an optimum at 2.55), where the CAT performs best due to a higher availability of protons. By increasing the **PTH** concentration at pH 2.55 to 2 mM (100 eq. relative to PS), we were able to further boost the TONs to a value of 20 660 with an average TOF of 3443 h^{-1} (over the course of 6 h; see also below Table 2 and Fig. 5b). This represents an enhancement factor of 3.1 relative to the reference system at pH = 4, or a factor of 11.3 relative to the reference system at pH = 2.55, regarding the TON and TOF after 6 h irradiation. These results show that **PTH** is able to act as a RM in this homogeneous HER photocatalytic system. In addition, time-dependent measurements were performed by measuring hydrogen evolution every hour within a time period of 6 h (Fig. S9 and Table S3). Thereby the RM-assisted system showed the overall same time-dependency trend as previously reported, with a diminishing of the catalytic activity over the irradiation time of 6 h.[33] Furthermore, add-back experiments were conducted (by a second addition of PS and CAT to the catalytic mixture after 6 h) showing that the RM-boosted system still outperforms the reference system at a pH of 2.55 and therefore is still active after 10.5 h (see SI, Fig. S10, Table S4).

Modification of phenothiazines

We next explored a range of substituted PT derivatives (**MPT**, **PEG-PT**, **TolPT-PEG**, **TolPT-diPEG**) as well as a polymer (**P1**) in order to investigate the general applicability of PTs' RM role and the effect of derivatization and partial improvement of water solubility (Fig. 3, for synthetic manipulations see the SI). The typical positions for introducing substituents in PT are the 3- and 7-positions on the aromatic core as well as the N-atom. The synthesized derivatives exhibited excellent solubility in a wide range of organic solvents and organic solvent/water mixtures, with moderate solubility in pure water. The only exception is derivative **TolPT-PEG**, which showed aggregation after a period of 6 h in the catalysis solvent mixture ($MeOH : H_2O$ (9 : 1, v : v)).

In addition to exhibiting an adequate solubility to perform homogeneous HER photocatalysis, the employed PT derivatives should have the following characteristics: (a) No strong light absorption within the wavelength range utilised for photocatalysis (*i.e.* 450 nm for $\{Ru\}^{2+}$ as PS), (b) a redox potential that falls between those of the excited-state redox potentials of the PS and the SED, and (c) an effective ability to reductively quench the photoexcited state of the PS. Consequently, UV/Vis-spectroscopy, cyclic voltammetry (CV) and Stern–Volmer-quenching experiments were conducted (Fig. 4). The data from the UV/Vis spectra and CV measurements are listed in Table 1 (for further information, see the SI).

UV/Vis spectra of neutral **PTH** and its derivatives show no absorption at the irradiation wavelength of 455 nm used in photocatalysis (Fig. 4a). The radical cations show an absorption in the UV region at 280 nm and in the visible range at 500–570 nm stemming from the radical cation itself (Fig. 4b).[25,43] In addition, the radical cations can interact either with a neutral PT molecule, leading to a so-called "pimer" (π-mer) with an absorption between 700–850 nm, or with another PT radical cation forming a "π-dimer" with a broad absorption at 1400 nm.[25] The absorption bands of the radical cations shift to higher wavelengths for the more electron-rich PT derivatives,

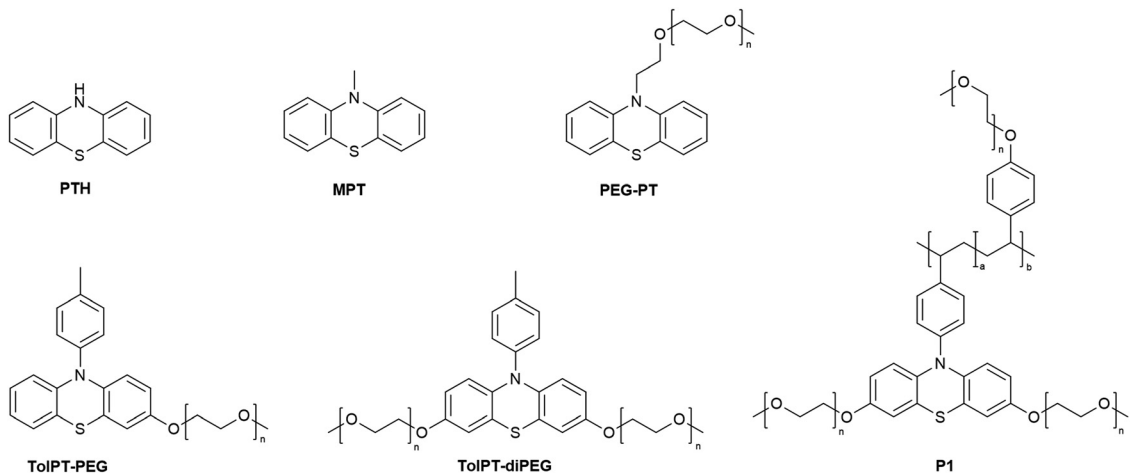

Fig. 3 Molecular structures of the PT derivatives herein investigated as RMs in photocatalytic HER.

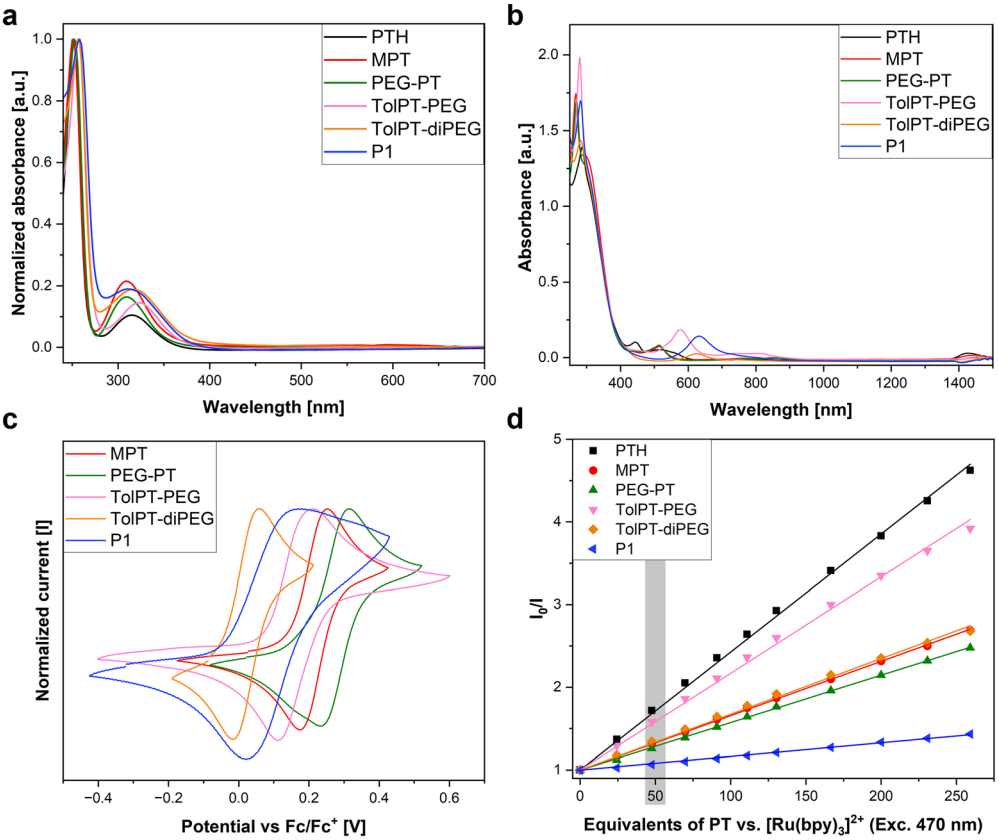

Fig. 4 UV/Vis, CV and emission quenching data of **PTH** and its derivatives. (a) Normalized UV/Vis spectra in MeOH : H_2O (9 : 1, v : v) at $c = 5 \times 10^{-5}$ M; (b) UV/Vis spectra of oxidized species (oxidizing agent: $(NH_4)_2[Ce^{(IV)}(NO_3)_6]$); (c) CVs in MeCN *vs.* Fc/Fc^+ (1 mM with 0.1 M *n*-Bu_4NPF_6, working and counter electrode: Pt, reference electrode: Ag/AgCl); (d) Stern–Volmer plots of the $\{Ru\}^{2+}$ emission quenching with **PTH** and derivatives (MeOH : H_2O (9 : 1, v : v); I_0/I: ratio of emission intensity after and before addition of a quencher).

Table 1 UV/Vis spectroscopic and cyclic voltammetry data of PTs

PT derivative	Absorption band/nm[a]	Absorption band of radical cation/nm[b]	First half-wave oxidation potential/V[c]
PTH	252*, 316	286*, 444, 520, 570, 740, 830, 1426	0.22[41,42]
MPT	252*, 308	268*, 292, 514, 764, 854, 1444	0.21
PEG-PT	252*, 308	270*, 514, 772, 866	0.27
TolPT-PEG	256*, 324	280*, 576, 736, 814	0.16
TolPT-diPEG	256*, 318	282*, 624, 732	0.03
P1	258*, 312	282*, 632, 728, 822	0.10

[a] In MeOH : H_2O (9 : 1, v : v) with $c = 1 \times 10^{-5}$ M. [b] In MeOH : H_2O (9 : 1, v : v) with $c = 1 \times 10^{-5}$ M, oxidizing agent: $(NH_4)_2(Ce^{(IV)}(NO_3)_6)$, absorption maximum marked with an asterisk. [c] *vs.* Fc/Fc^+ in MeCN with $c = 1 \times 10^{-3}$ M using 0.1 M *n*-Bu_4NPF_6 (working and counter electrode: Pt, reference electrode: Ag/AgCl), half-wave potential of **PTH** calculated according to Pavlishchuk *et al.*[42]

from 444 nm (**PTH**) to 624 nm (**TolPT-diPEG**) and 632 nm (**P1**). In addition, the formation of the π-dimer is more pronounced for the smaller PT derivatives and diminishes for the more sterically hindered derivatives, since the interaction of the obtained radical cations is suppressed. The same trend can be seen for the π-mer formation. The UV/Vis spectra of the neutral PT derivatives hence do not interfere with the used irradiation wavelength (455 nm). For the oxidized PT derivatives, a slight overlap of the used irradiation wavelength and the absorption of the radical cation is possible, however within the scope of this study no impact of the absorption overlap on the catalytic performance could be elucidated.

The CV measurements showcase the ability of the PT derivatives to act as RMs within the catalytic cycle with half-wave potentials in the range of 0.03–0.27 V in MeCN (*vs.* Fc/Fc^+, Fig. 4c and Table 1). With $E_{red.}^{1/2}$ ($Ru^{2+*/1+}$) = 0.39 V in MeCN (*vs.* Fc/Fc^+) obtained from Prier *et al.*[44] and adjusted according to Pavlishchuk *et al.*,[42] the redox potential of the excited PS $\{Ru\}^{2+*}$ lies higher, and with $E_{ox.}^{1/2} \approx 0.08$ V in H_2O (*vs.* Fc/Fc^+), obtained from Pellegrin *et al.*[45] and adjusted according to Pavlishchuk *et al.*,[42] the redox potential of the SED HAsc lies at a lower value.

The Stern–Volmer plots of the emission quenching experiments of the $\{Ru\}^{2+}$ PS by the PT derivatives in Fig. 4d show that all PT derivatives are able to quench the emission of the Ru complex, with the order of efficiency **PTH** ≫ **TolPT-PEG** ≫ **TolPT-diPEG** ≅ **MPT** > **PEG-PT** ≫ **P1**. Important to note is that the quenching in all cases (except for the polymer **P1**) for 50 eq. PT derivative to PS is higher than that achieved with HAsc (500 eq. to PS), which shows that the PT derivatives can indeed serve as RMs in the photocatalytic cycle, as proposed in Fig. 1b,

efficiently reducing the photoexcited state of $\{Ru\}^{2+}$ (see SI, Fig. S1).

We next tested the PT derivatives in photocatalytic HER, as described above for **PTH**. The proposed photocatalytic cycle is shown in Fig. 5a and starts with a photoexcitation of the PS $\{Ru\}^{2+}$, followed by its reductive quenching, forming $\{Ru\}^{+}$. $\{Ru\}^{+}$ reduces the $\{Mo_3\}^{2-}$ CAT, which accepts a proton from solution and forms $H[Mo_3S_{13}]^{2-}$. A second electron/proton transfer to CAT results in formation of H_2 and regeneration of the native $\{Mo_3\}^{2-}$ species (see green box in Fig. 5a). As demonstrated above by adding **PTH** to the "reference" system (Fig. 2b), it acts as an RM (highlighted with the blue box) and takes over the part of reductive quenching of the photoexcited PS. The thereby formed radical cation ($PT^{\bullet+}$) is then re-reduced by Asc^- as SED and therefore acts catalytically as RM (SI, Fig. S3).

As is evident from the photocatalytic cycle in Fig. 5a, the pH value and consequently the concentration of protons is a decisive factor. When using $\{Ru\}^{2+}$ as PS and a Ni-phosphine complex as CAT, Durrant *et al.*[16] showed that the catalyst performed best at acidic (low) pH, since this accelerates the protonation step of the reduced catalyst.[16,34] The PS, on the other hand, performed better at higher pH values, which can be explained by the easier oxidation of Asc^- compared to HAsc.[16] While for the $\{Mo_3\}^{2-}$ CAT, the optimal operating conditions were reported to be at pH 4,[33] we showed above that with **PTH** as RM the best pH is at 2.55 (Fig. 5b and Table 2).

The same trend we observed for the PT derivatives, with TONs shown in Fig. 5b after 6 h reaction time upon varying the pH of the aqueous photocatalytic solution, employing a 1 mM concentration of the respective PT derivative (corresponding to 50 eq. to PS and 3.33×10^3 eq. with respect to CAT). We adjusted the pH of the aqueous solution to values between 0.85 and 4 using H_3PO_4 as acid and NaOH or NH_4OH as base (Table 2). The optimal pH was found to be 2.55 delivering the highest TONs, which is the pH of the HAsc stock solution, making it practically feasible. Here, we obtained the highest TON of 16 500 ± 1500 with **PTH** as RM for 50 eq. used with respect to the PS (black dots in Fig. 5b). We could further boost the TONs by using 100 eq. of **PTH** relative to PS to 20 660 ± 4000 (see Table 2), corresponding to an enhancement by a factor of 3.1 compared to the $(NH_4)_2\{Mo_3\}$ system (purple square in Fig. 2b) at pH 4. *N*-Methylphenothiazine (**MPT**) performed second-best with a TON of 12 800 ± 3500 at pH 2.55 (red triangles), followed by *N*-pegylated PT (**PEG-PT**) (green triangles) with a TON of 5720 ± 1400.

Further acidification using H_3PO_4 resulted in a decrease in TON, indicating that anionic Asc^- is required to re-reduce the PT radical cations formed upon ET with PS. Nevertheless, the system continues to effectively function under highly acidic conditions, a property that renders it potentially valuable for a range of further applications. At the most acidic pH of 1.25, the order of performance was **MPT** > **PTH** > **PEG-PT** > **TolPT-PEG** > **TolPT-diPEG** ≅ **PTPT-diPEG** with a TON for **MPT** of 8520 ± 800. **TolPT-PEG**, **TolPT-diPEG** and **PTPT-diPEG** also functioned as RMs at pH <3 but did not boost the HER beyond the TONs obtained for the reference system. Of molar ratios

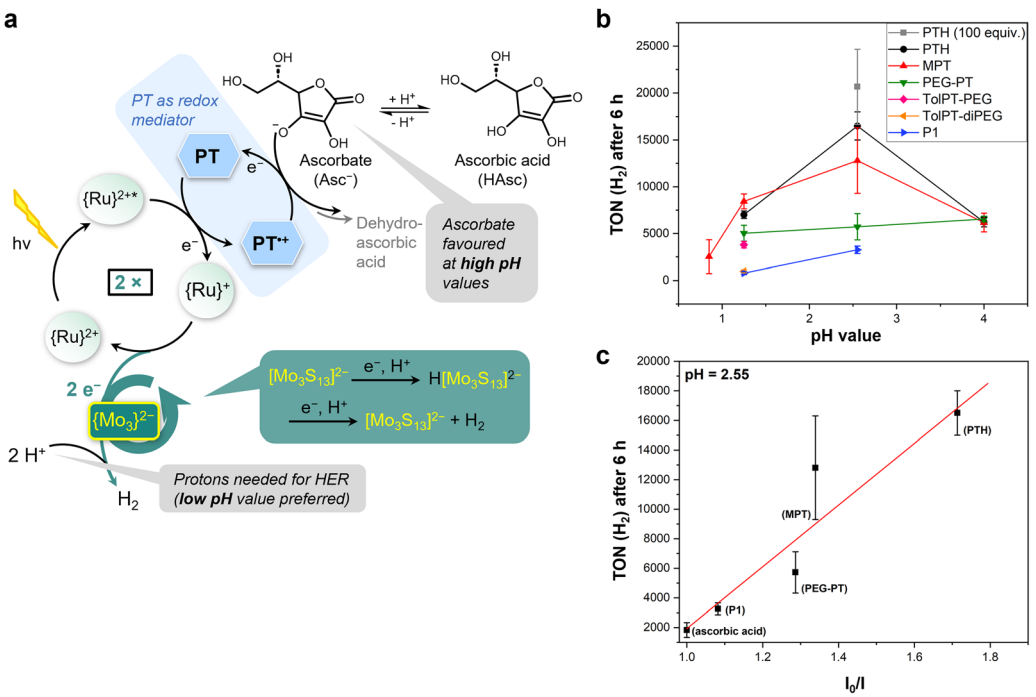

Fig. 5 (a) Schematic representation using PTs as RMs in the photocatalyzed HER with $\{Mo_3\}^{2-}$ as CAT, $\{Ru\}^{2+}$ as PS, with grey boxes highlighting the influence of the pH value. (b) Averaged TONs after 6 h at different pH using different PT derivatives as RM (1 mM; with 0.3 μM $(NH_4)_2\{Mo_3\}$, 20 μM $\{Ru\}^{2+}$, 10 mM HAsc in MeOH : H_2O (9 : 1, v : v)), irradiation at 455 nm). (c) Correlation between the average TONs (at pH 2.55) and the excited-state quenching ability of the PT RMs towards photoexcited $\{Ru\}^{2+}$ for 50 eq. of quencher. Note: Measurements were carried out at (21 ± 1) °C. I_0/I: ratio of emission intensity before and after addition of the quencher.

Table 2 Average TONs[a] (each determined as triplicates) for the photocatalyzed HER using $\{Mo_3\}^{2-}$ as CAT, $\{Ru\}^{2+}$ as PS, HAsc as SED, PT and its derivatives as RMs at different pH-values

pH of aqueous stock solution	0.85 (adj. with H_3PO_4)	1.25 (adj. with H_3PO_4)	2.55	4 (adj. with NH_4OH[b] or NaOH[c])
Reference (without PT derivative)	—	140 ± 30	1830 ± 500	6760 ± 400[b]
PTH	—	7010 ± 400	16 500 ± 1500 *20 660 ± 4000	6220 ± 500[b]
MPT	2540 ± 1800	8520 ± 800 *10 700 ± 2000	12 800 ± 3500	6170 ± 1000[c]
PEG-PT	—	5030 ± 850 *8490 ± 2500	5720 ± 1400	6550 ± 300[c]
TolPT-PEG	—	3800 ± 350	—	—
TolPT-diPEG	—	980 ± 150	—	—
P1	—	790 ± 150	3260 ± 400	—

[a] Conditions: $(NH_4)_2\{Mo_3\}$ (0.3 μM), $\{Ru\}^{2+}$ (20 μM), HAsc (10 mM), **PTH** or derivative (1 mM = 50 eq. to PS) in MeOH : H_2O (9 : 1, v : v), 2 mL; irradiation at 455 nm for 6 h; * **PTH** or derivative (2 mM = 100 eq.).

between 12.5 and 200 eq. we obtained the best performance at 100 eq., corresponding to a concentration of 2 mM RM (see SI, Fig. S8). The decrease in TON for higher PT derivative concentrations could be due to an accumulation of the corresponding PT radical cations, which can intercept the electron cascade needed for hydrogen production. The overall acidification of the catalytic solution and the overall low concentration of PT derivatives has the additional benefit of slowing down the disproportionation of PT radical cations (second-order kinetics), as shown in aqueous systems reported for similar PT motives by Ishchenko *et al.*[46] ^{1}H-NMR and GC-MS/MALDI-TOF measurements indicated no signs of decomposition of the PT derivatives after a period of 6 h irradiation at pH 1.25 using 50 eq. PT with respect to PS (see SI, Fig. S36–S51).

We next investigated a potential correlation between the fluorescence quenching efficiency of $\{Ru\}^{2+}$ emission by the PT RMs and the photocatalytic performance. Fig. 5c shows the TONs obtained at pH 2.55 (see Table 2) as a function of the Stern–Volmer-quenching constant obtained at a ratio of 50 eq. of PT RM to $\{Ru\}^{2+}$. A correlation is clearly visible, with the TON increasing with rising quenching efficiency. We thus propose that the initial reductive quenching of the Ru-PS excited state by the PT RM is an important kinetic factor in the catalytic cycle. This would explain the fact that a RM with more efficient reductive quenching ability compared to the SED is able to significantly enhance the TONs of this HER.

Conclusions

In summary, we herein show that phenothiazine and derivatives can act as redox mediators (RMs) in the homogeneous photocatalytic hydrogen-evolution reaction (HER), by performing the reductive quenching of the photosensitizer instead of a sacrificial electron donor (SED). By using the thiomolybdate cluster $(NH_4)_2[Mo_3S_{13}]$ ($(NH_4)_2\{Mo_3\}$) as hydrogen-evolution catalyst and $[Ru(bpy)_3]^{2+}$ ($\{Ru\}^{2+}$) as PS, both phenothiazine and its derivatives effectively quench the photoexcited state of the $\{Ru\}^{2+}$ PS through electron transfer, forming the corresponding radical cation $PT^{\bullet+}$. The reduced PS then reduces the $\{Mo_3\}^{2-}$ catalyst, which – upon two-electron transfers – produces hydrogen from a proton source. The oxidized phenothiazine derivatives are re-reduced by Asc^-/HAsc as SED. Remarkably, this photocatalytic system operates well at acidic pHs with an optimum at 2.55 at which a higher concentration of protons is available for the HER catalysis compared to the best literature-reported conditions at pH 4. This significantly increases the TONs to up to 20 660 ± 4000 and the TOF from 1130 h^{-1} to 3440 h^{-1} (after 6 h), both corresponding to a factor of three compared to the best RM-free $(NH_4)_2\{Mo_3\}$ system (at pH 4).

We observed a near-linear correlation between the fluorescence-quenching efficiency of the $\{Ru\}^{2+}$ PS emission by the PT RM and the photocatalytic performance, which showed that the initial quenching of the PS excited state by the redox mediator is an important kinetic factor within the photocatalytic cycle. Our study demonstrates a pathway to boost photocatalytic HER systems by using low-pH-compatible RMs enabling more acidic conditions in artificial photosynthesis. Overall, the presented system utilizing the PT-based RM benefits from the formation of the reductively quenched photosensitizer through a pH-independent reductive quenching step. This leads to a more efficient electron cascade at lower pH values, effectively boosting the HER in this pH window.

More generally, it should be noted that photocatalytic processes often show turnover frequencies on the min-timescale whereas the photochemical processes to activate the catalyst typically occur on the ms-to-s timescale. This discrepancy highlights that the bottleneck of photocatalytic processes often lies in the inefficient substrate conversion at the catalyst. Thus, providing higher substrate concentrations (*i.e.* protons for HER) is a way forward to not only accelerate photocatalytic HER but also to ultimately derive meaningful structure–property relationships of photocatalytic HER systems and with it the advancement of this research field. If the best-optimized photocatalytic systems are hampered by substrate conversion at the catalyst resulting in comparable TONs as non-optimized systems, a TON-driven rational system development is impossible.

This SED/RM-combination could not only be applied to many other homogeneous HER systems that suffer from CAT-limited low H_2 output due to pH limitations for commonly used SEDs but it also paves the way for coupling reductive and oxidative photocatalysis by using redox mediators with

reversible redox chemistry instead of sacrificial electron donors (or acceptors).

Author contributions

Conceptualization: B. E., D. B., S. R.; data curation: All authors; synthesis of PT derivatives: D. B., M. G.; synthesis of catalyst: Y. G., M. J.; investigation: D. B., M. G.; formal analysis: D. B., M. G.; methodology: All authors; funding acquisition: B. E., C. S., S. R.; project administration: B. E.; resources: B. E., C. S., S. R.; supervision: B. E.; validation: All authors; visualization: B. E., D. B.; writing – original draft: B. E., D. B.; writing – review & editing: all authors.

Conflicts of interest

There are no conflicts to declare.

Data availability

The data obtained in this study have been deposited in the repository Zenodo and are available under the digital object identifier: DOI: https://doi.org/10.5281/zenodo.17799373.

Supplementary information (SI): materials and methods, Stern–Volmer quenching experiments, UV/Vis/NIR spectra, details on HER experiments, results on varying the equivalents of PT to $\{Ru\}^{2+}$, time-dependant HER and add-back experiments, synthetic procedures, NMR spectra, ''post-mortem'' analyses, exemplary GC-traces of hydrogen detection. See DOI: https://doi.org/10.1039/d6ey00029k.

Acknowledgements

Financial support by the Deutsche Forschungsgemeinschaft (DFG, German Research Foundation) – project numbers 364549901 (SFB/TRR 234 ''CataLight'', projects A1, A5, A6 and B3), 445471097, 445471845 and 528773185 – is gratefully acknowledged.

Notes and references

1 D. G. Nocera, *Inorg. Chem.*, 2009, **48**, 10001–10017.
2 N. S. Lewis and D. G. Nocera, *Proc. Natl. Acad. Sci. U. S. A.*, 2006, **103**, 15729–15735.
3 H. B. Gray, *Nat. Chem.*, 2009, **1**, 7.
4 R. Nersesian, *Energy Technol.*, 2014, **2**, 215.
5 E. Connelly, M. Penev, A. Milbrandt, B. Roberts, N. Gilroy and M. Melaina, *Resource Assessment for Hydrogen Production*, National Renewable Energy Laboratory (NREL), Golden, CO (United States), 2020.
6 B. Reda, A. A. Elzamar, S. AlFazzani and S. M. Ezzat, *Environ. Dev. Sustainable*, 2025, **27**, 29213–29233.
7 M. Kirch, J. Lehn and J. Sauvage, *Helv. Chim. Acta*, 1979, **62**, 1345–1384.
8 B. König, *Chemical Photocatalysis*, Walter de Gruyter GmbH, Berlin/Boston, 2nd edn, 2020.
9 F. Droghetti, F. Lucarini, A. Molinari, A. Ruggi and M. Natali, *Dalton Trans.*, 2022, **51**, 10658–10673.
10 K. E. Dalle, J. Warnan, J. J. Leung, B. Reuillard, I. S. Karmel and E. Reisner, *Chem. Rev.*, 2019, **119**, 2752–2875.
11 Y. Halpin, M. T. Pryce, S. Rau, D. Dini and J. G. Vos, *Dalton Trans.*, 2013, **42**, 16243.
12 Y.-J. Yuan, Z.-T. Yu, D.-Q. Chen and Z.-G. Zou, *Chem. Soc. Rev.*, 2017, **46**, 603–631.
13 M. Z. Rahman, M. G. Kibria and C. B. Mullins, *Chem. Soc. Rev.*, 2020, **49**, 1887–1931.
14 S. Losse, J. G. Vos and S. Rau, *Coord. Chem. Rev.*, 2010, **254**, 2492–2504.
15 R. S. Khnayzer, V. S. Thoi, M. Nippe, A. E. King, J. W. Jurss, K. A. El Roz, J. R. Long, C. J. Chang and F. N. Castellano, *Energy Environ. Sci.*, 2014, **7**, 1477–1488.
16 A. Reynal, E. Pastor, M. A. Gross, S. Selim, E. Reisner and J. R. Durrant, *Chem. Sci.*, 2015, **6**, 4855–4859.
17 J. Barber, *Q. Rev. Biophys.*, 2003, **36**, 71–89.
18 D. Shevela, J. F. Kern, G. Govindjee, J. Whitmarsh and J. Messinger, in *Encyclopedia of Life Sciences*, Wiley, 1st edn, 2021, pp. 1–16.
19 F. Baskoro, S. U. Sharma, A. L. Lubis and H.-J. Yen, *J. Mater. Chem. A*, 2025, **13**, 1552–1589.
20 J. A. Kowalski, M. D. Casselman, A. P. Kaur, J. D. Milshtein, C. F. Elliott, S. Modekrutti, N. H. Attanayake, N. Zhang, S. R. Parkin, C. Risko, F. R. Brushett and S. A. Odom, *J. Mater. Chem. A*, 2017, **5**, 24371–24379.
21 Y. Yan, D. B. Vogt, T. P. Vaid, M. S. Sigman and M. S. Sanford, *Angew. Chem., Int. Ed.*, 2021, 60, 27039–27045.
22 C. Zhang, Z. Niu, S. Peng, Y. Ding, L. Zhang, X. Guo, Y. Zhao and G. Yu, *Adv. Mater.*, 2019, **31**, 1901052.
23 M. Banerjee and A. Anoop, *Chem. – Eur. J.*, 2024, **30**, e202304206.
24 R. Gavale, M. Ghasemi, F. Khan, D. Volyniuk, J. V. Grazulevicius and R. Misra, *J. Mater. Chem. C*, 2024, **12**, 2134–2147.
25 B. Esser, I. H. Morhenn and M. Keis, *Acc. Mater. Res.*, 2025, **6**, 754–764.
26 X. Li, B. Liu, M. Wen, Y. Gao, H. Wu, M. Huang, Z. Li, B. Chen, C. Tung and L. Wu, *Adv. Sci.*, 2016, **3**, 1500282.
27 K. Wu, Y. Du, H. Tang, Z. Chen and T. Lian, *J. Am. Chem. Soc.*, 2015, **137**, 10224–10230.
28 A. Indra, R. Beltrán-Suito, M. Müller, R. P. Sivasankaran, M. Schwarze, A. Acharjya, B. Pradhan, J. Hofkens, A. Brückner, A. Thomas, P. W. Menezes and M. Driess, *ChemSusChem*, 2021, **14**, 306–312.
29 G. Yang, L. Blechschmidt, L. Zedler, C. Zens, K. Witas, M. Schmidt, B. Esser, S. Rau, G. E. Shillito, B. Dietzek-Ivanšić and S. Kupfer, *Chem. – Eur. J.*, 2025, **31**, e202404671.
30 S. Batool, M. Langer, S. N. Myakala, M. Heiland, D. Eder, C. Streb and A. Cherevan, *Adv. Mater.*, 2024, **36**, 2305730.
31 M. Dave, A. Rajagopal, M. Damm-Ruttensperger, B. Schwarz, F. Nägele, L. Daccache, D. Fantauzzi, T. Jacob and C. Streb, *Sustainable Energy Fuels*, 2018, **2**, 1020–1026.

32 S. Batool, M. Langer, S. N. Myakala, M. Heiland, D. Eder, C. Streb and A. Cherevan, *Adv. Mater.*, 2024, **36**, 2305730.
33 M. Heiland, R. De, S. Rau, B. Dietzek-Ivansic and C. Streb, *Chem. Commun.*, 2022, **58**, 4603–4606.
34 P. D. Tran, T. V. Tran, M. Orio, S. Torelli, Q. D. Truong, K. Nayuki, Y. Sasaki, S. Y. Chiam, R. Yi, I. Honma, J. Barber and V. Artero, *Nat. Mater.*, 2016, **15**, 640–646.
35 J. Zanzi, Z. Pastorel, C. Duhayon, E. Lognon, C. Coudret, A. Monari, I. M. Dixon, Y. Canac, M. Smietana and O. Baslé, *JACS Au*, 2024, **4**, 3049–3057.
36 S. M. Sartor, C. H. Chrisman, R. M. Pearson, G. M. Miyake and N. H. Damrauer, *J. Phys. Chem. A*, 2020, **124**, 817–823.
37 Y. Luo, J. H. Tran, M. Wächtler, M. Schulz, K. Barthelmes, A. Winter, S. Rau, U. S. Schubert and B. Dietzek, *Chem. Commun.*, 2019, **55**, 2273–2276.
38 Y. Luo, K. Barthelmes, M. Wächtler, A. Winter, U. S. Schubert and B. Dietzek, *Chem. – Eur. J.*, 2017, **23**, 4917–4922.
39 G. Ajayakumar, K. Sreenath and K. R. Gopidas, *Dalton Trans.*, 2009, 1180–1186.
40 D. Kowalczyk, P. Li, A. Abbas, J. Eichhorn, P. Buday, M. Heiland, A. Pannwitz, F. H. Schacher, W. Weigand, C. Streb and D. Ziegenbalg, *ChemPhotoChem*, 2022, **6**, e202200044.
41 V. Novakova, P. Hladík, T. Filandrová, I. Zajícová, V. Krepsová, M. Miletin, J. Lenčo and P. Zimcik, *Phys. Chem. Chem. Phys.*, 2014, **16**, 5440.
42 V. V. Pavlishchuk and A. W. Addison, *Inorg. Chim. Acta*, 2000, **298**, 97–102.
43 K. Minakata, O. Suzuki, Y. Ishikawa, H. Seno and N. Harada, *Forensic Sci. Int.*, 1992, **52**, 199–210.
44 C. K. Prier, D. A. Rankic and D. W. C. MacMillan, *Chem. Rev.*, 2013, **113**, 5322–5363.
45 Y. Pellegrin and F. Odobel, *C. R. Chim.*, 2016, **20**, 283–295.
46 R. Ishchenko, M. Becuwe, L. Dubois, S. Gambarelli, C. Cézard and E. Baudrin, *ChemistryEurope*, 2025, **3**, e202500226.